JCTC Journal of Chemical Theory and Computation

Article

pubs.acs.org/JCTC

# Robustness of Frequency, Transition Dipole, and Coupling Maps for Water Vibrational Spectroscopy

S. M. Gruenbaum,* C. J. Tainter, L. Shi, Y. Ni, and J. L. Skinner

Theoretical Chemistry Institute and Department of Chemistry, 1101 University Ave., University of Wisconsin-Madison Madison, Wisconsin 53706, United States

**ABSTRACT:** Infrared spectroscopy of the water OH stretch provides a sensitive probe of the local hydrogen-bonding structure and dynamics of water molecules. Previously, we have utilized a mixed quantum/classical model to calculate vibrational spectroscopic observables for bulk water, ice, the liquid/vapor interface, and small water clusters, as well as water interacting with ions and biological molecules. These studies rely on spectroscopic maps that relate the OH stretching frequency and transition dipole to the local environment around a water molecule. Our spectroscopic maps were parametrized based on water clusters taken from bulk water simulations; in this article, we test the robustness of these maps for water in nonbulk-liquid environments. We find that the frequency, transition dipole, and coupling maps work as well for the water surface, ice Ih, and the water hexamer as they do for liquid water. This suggests that these maps may be generally applied to study the vibrational spectroscopy of water in diverse, potentially heterogeneous environments.

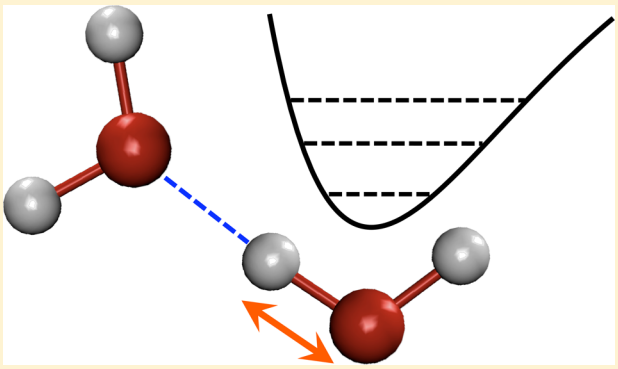

## I. INTRODUCTION

Water is ubiquitous in many areas of chemistry and biology, and there is a great deal of scientific interest in understanding how and why the properties of water are altered in different environments. For example, the rotational and diffusive motion of water molecules hydrating proteins, DNA, and lipid membranes can be significantly slower than in bulk water,[1−13] while the dynamics of hydrogen-bond rearrangement at the liquid/vapor interface is quite distinct from that in the bulk.[14−21] Due to the sensitivity of the water OH stretching frequency to its environment, vibrational infrared (IR) spectroscopy of this mode provides a useful probe of the local hydrogen-bonding structure around a water molecule.[22−26] In addition to such structural information, nonlinear techniques such as two-dimensional infrared (2DIR)[27−35] and anisotropic pump−probe spectroscopy[36−41] can probe spectral diffusion dynamics and reorientational motion[42,43] on the picosecond time scale. Finally, surface-sensitive techniques such as sum-frequency generation (SFG) spectroscopy have been used to investigate the orientation of water molecules at interfaces.[44−48]

While vibrational spectroscopy is a powerful tool for understanding both structure and dynamics, the proper interpretation of the experimental results is sometimes ambiguous.[49−53] To complement experiment, molecular dynamics simulations have been utilized by many groups to directly obtain the thermodynamic, structural, and dynamical properties of water molecules in many different environments.[10,54−61] We and others have tried to furnish a link between simulation and experiment by calculating spectroscopic observables directly from computer simulation trajectories. Previously, we have utilized a mixed quantum/classical approach,[62] where the low-frequency degrees of freedom are treated classically through molecular dynamics simulation, and the spectroscopic (OH stretch) degrees of freedom are treated quantum mechanically. Within this picture, the OH stretches are conveniently described by a vibrational exciton Hamiltonian in the local-mode basis.[63,64] The diagonal elements of the Hamiltonian are the local-mode transition frequencies, and the off-digaonal elements are the vibrational couplings between local modes (these could be intramolecular or intermolecular). The exciton Hamiltonian fluctuates as the classical degrees of freedom evolve in time. From this fluctuating Hamiltonian, one can calculate spectroscopic observables.[65]

The key to the success of this approach is the accurate description of the exciton Hamiltonian for a given configuration of the classical variables. This is a problem that quantum chemistry can solve, in principle, on the fly. In practice, however, that would be computationally too expensive. Instead, we perform electronic structure calculations for a reasonably small number of clusters extracted from a simulation of liquid water[66] to develop a set of "maps", which are parametrized to provide the frequencies and couplings of the exciton Hamiltonian (and also the transition dipole moment) as a function of the nuclear positions. The maps have been used by our group to calculate a number of linear and nonlinear spectroscopic observables for liquid water,[67−70] while Jansen et

Received: April 9, 2013
Published: June 5, 2013

  

al. have utilized these maps to study the 2DIR spectroscopy of water in an acetonitrile solvent.[71] The maps have in addition been used in calculations for ice,[72−75] the liquid/vapor interface,[21,48,51] water clusters,[76] salt solutions,[77] and hydration water around membranes and in reverse micelles.[12,13,78] Similar mapping strategies incorporating both electric fields and electric field gradients have also been successfully used by Mukamel and co-workers to simulate water vibrational spectroscopy.[79−81] Each of these studies brings up the question: how well do these maps, which were parametrized for liquid water, work for water in other kinds of environments? If the configurations in liquid water were representative of water in these other situations, then one would expect that the maps would work well. However, it is not obvious that this is the case. For example, water in ice and the water hexamer have specific kinds of hydrogen bonds,[82] not necessarily typical of the liquid, while water at the liquid surface has a much larger fraction of lower-coordinated molecules and "free OHs". The purpose of this article is to assess the robustness of these maps.

Substitution of hydrogen with deuterium lowers the OH stretch frequency by almost 1000 $cm^{-1}$, which effectively decouples OD from OH stretches. Experimentalists exploit this fact, considering for example dilute HOD in $H_2O$ or $D_2O$, and focusing on the OD or OH stretch, respectively.[26] In addition, Bakker and co-workers have studied $D_2O/H_2O$ mixtures to probe vibrational energy transfer.[36,39,41] To understand these experiments, it is thus important to develop OD-stretch as well as OH-stretch maps. For nonlinear experiments the two-exciton manifold is excited, and so, it is also necessary to describe this block of the exciton Hamiltonian. Finally, it is important to note that different simulation models have different charges and molecular geometries for the water molecule. Since our maps involve the electric field from these charges, different simulation models will, in principle, require different maps. Thus, for example, we have published both SPC/E and TIP4P maps.[67−69,72,73] In recent years, we have mostly studied the E3B water model—a rigid model with explicit three-body interactions.[83,84] This model uses TIP4P as its two-body reference, and so, the electric field from an E3B water molecule is identical to that from a TIP4P water molecule. Therefore, to the extent that the configurations generated from a TIP4P liquid simulation are representative of those from an E3B liquid simulation, we should be able to use TIP4P maps in conjuction with the E3B simulation model. In this paper, we will also explicitly test this supposition.

Whether we are developing the maps for the liquid, or testing them for water in other situations, for a collection of water molecules we use electronic and nuclear quantum mechanics to calculate the local OH-stretch transition frequencies, the transition dipoles, and the vibrational couplings. Our methods for doing so are described in section II. In section III, we then review, update, and complete our set of OH and OD TIP4P maps. In section IV, we will show that these TIP4P maps work well for E3B water in the bulk liquid, the liquid surface, ice, and the hexamer. In section V, we conclude, including a short discussion as to why the electric-field maps work as well as they do.

## II. GENERATION OF CLUSTERS AND QUANTUM CHEMICAL CALCULATIONS

As described in section I, for the development of TIP4P maps we extract clusters of water molecules from a liquid-state simulation of TIP4P water. For the testing of the maps on E3B water in the bulk liquid, in ice, at the liquid surface, and in the hexamer, we also have to run molecular dyamics simulations and extract configurations. For each water cluster, we then need to calculate local OH-stretch frequencies, transition dipoles, and vibrational coupling. We use electronic and nuclear quantum mechanics to do so.

Simulations of bulk water, ice Ih, the liquid/vapor interface, and the water hexamer using the newly developed E3B water force field,[83,84] as well as bulk water simulations using the TIP4P force field,[85] were performed with a modified version of the GROMACS package.[86] For both E3B and TIP4P bulk water simulations, 887 water molecules were simulated in the NPT ensemble at a temperature of 300 K and a pressure of 1 bar.[87,88] Electrostatic interactions were treated with the particle-mesh Ewald method,[89] Lennard-Jones interactions were truncated at a cutoff of 1 nm, and we used a time-step of 1 fs. As described previously, ice Ih simulations were similarly performed with 432 molecules at temperatures of 10, 100, and 245 K,[75] while the liquid/vapor interface was simulated at 300 K with 500 molecules in a slab geometry.[21] Configurations were also taken from replica-exchange molecular dynamics simulations of the water hexamer at both 80 and 194 K.[76]

In order to calculate the environmental dependence of the OH (or OD) stretching frequency and dipole derivative, clusters of water molecules centered on a randomly chosen water hydrogen atom were selected from each molecular dynamics simulation described (except that for the hexamer we always consider all six molecules). We then systematically stretched and contracted the central OH bond of interest and mapped out a one-dimensional potential energy surface using the Gaussian software package.[90] For our density functional theory (DFT) calculations (see below), all water molecules whose oxygen was within a cutoff of 4.0 Å of the central hydrogen atom were explicitly included in the calculation, while all waters between 4.0 and 7.831 Å were implicitly included only as point charges (for both TIP4P and E3B water, each hydrogen atom is given a charge of $+0.52e$, while a charge of $-1.04e$ is placed on the dummy atom M site).[85] For calculations of ice, the explicit cutoff was extended to 4.15 Å in order to match the minimum in the ice OH radial distribution function. Clusters for the liquid/vapor interface were chosen such that the central water molecule was a "surface" molecule based on the definition described by Ni et al.[21] For the hexamer, all six water molecules were treated explicitly. For bulk water, we have tested the effect of changing the explicit cutoff value, and it was found that increasing the cutoff up to 5 Å did not significantly affect the calculated OH stretching frequencies, though it did dramatically increase the computational time. Changing the implicit cutoff value has only a minimal effect on the resulting frequencies.

For each water cluster, the central OH bond length was varied between 0.6572 and 1.7572 Å with a grid spacing of 0.02 Å. The coordinates of the center of mass (and the bond angle and the other bond length) of this central water molecule were fixed as the bond was stretched, and all other explicit and implicit water molecules were not moved from the positions obtained from the molecular dynamics simulation. At each bond length, both the total energy and dipole moment of the system were calculated using DFT within the B3LYP functional and the 6-311++G** basis set.[91] Note that we also explored many other functionals, including dispersion-corrected functionals,[92] and found that B3LYP predicts a potential energy curve for the OH stretch that is in good agreement with the

coupled cluster CCSD(T) result for the water monomer and dimer.

From the resulting potential energy surface, the 1−0 and 2−1 stretching frequencies $\omega_{10}$ and $\omega_{21}$ were then computed using the discrete variable representation (DVR) method of Colbert and Miller.[93] For this purpose, we assumed that the water molecule was actually HOD, which was treated as a pseudodiatomic with the appropriate H and OD (or D and OH in the case of the OD stretch) masses. When we perform this procedure on the HOD monomer, we obtain OH and OD stretch frequencies of 3699 and 2723 $cm^{-1}$, respectively, which can be compared with the experimental results of 3707 and 2727 $cm^{-1}$.[94] The agreement between theory and experiment must to some extent be fortuitous, with cancellation arising from different errors in the theoretical calculation (one-dimensional and pseudodiatomic approximations; imperfect level of electronic structure and basis set). Although it is probably unecessary, to account for these small differences, we multiply all calculated transition frequencies by scale factors of 1.0021 and 1.0016 for the OH and OD stretch, respectively.

For spectroscopic calculations, we also need the coordinate and momentum matrix elements,[62] which were calculated with the DVR method, and the dipole derivative, $\mu'$, which was calculated numerically from the slope (with respect to a changing OH stretch coordinate) of the total dipole moment at the equilibrium bond distance.

As described previously,[73,74] the intramolecular coupling between two OH chromophores $j$ and $k$ on the same molecule is given by

$$\hbar\omega_{jk}^{\text{intra}} = k_{jk}^{\text{intra}} x_j x_k + \frac{\cos\phi}{m_O} p_j p_k \tag{2.1}$$

where $x_j$ and $p_j$ are the 1−0 coordinate and momentum matrix elements of chromophore $j$ respectively, $\phi$ is the TIP4P (or E3B) HOH angle of 104.52°, $m_O$ is the oxygen mass, and $k_{jk}^{\text{intra}}$ is the second derivative of the potential energy surface with respect to both bond lengths, evaluated at the equilibrium bond distances. Likewise, the intermolecular coupling is simply

$$\hbar\omega_{jk}^{\text{inter}} = k_{jk}^{\text{inter}} x_j x_k \tag{2.2}$$

where $k_{jk}^{\text{intra}}$ is again the second derivative of the potential energy surface. In order to calculate $k_{jk}^{\text{intra}}$ and $k_{jk}^{\text{intra}}$, we selected water clusters from molecular dynamics simulations as described above and then numerically determined the two-dimensional potential energy surface due to stretching and contracting two OH bonds. For the intramolecular case, all water molecules within 4.07 Å of the central water oxygen were included explicitly in DFT calculation, while waters within 7.831 Å were again included only as charges. For intermolecular couplings, pairs of molecules were defined by choosing a hydrogen atom at random and then determining the closest oxygen atom. At that point, one OH bond on each of these two molecules was chosen at random. All water molecules within 4.0 Å of either hydrogen (4.15 Å for ice) were included explicitly in the calculation, while all other molecules within 7.831 Å of either hydrogen were included as charges. For both the intra- and intermolecular cases, each OH bond length was varied between 0.9322 and 1.0322 Å, with a grid spacing of 0.0025 Å. The second derivative of the potential energy surface was then computed numerically around the energy minimum.

## III. COMPLETE SET OF REVISED AND UPDATED TIP4P MAPS

In this section, we use the calculated transition frequencies, dipoles, and vibrational couplings from TIP4P liquid water configurations to parametrize a set of maps. Previously, we have reported several such sets of maps for both the water OH and OD stretch, parametrized from water clusters chosen from bulk water simulations using both the SPC/E[68,69] and TIP4P[72,73] force fields. More recently, we have presented an updated dipole derivative map for TIP4P water[75] as well as OD stretch maps for the frequency and coordinate matrix element between the first and second excited states, $\omega_{21}$ and $x_{21}$.[21] Using the methods described in section II, herein we complete our set of maps by calculating $\omega_{21}$ and $x_{21}$ for the water OH stretch as well as momentum matrix element maps $p_{21}$ for both the OD and OH stretches.

Our spectroscopic maps yield, for example, the transition frequency given a particular local environment around a water OH stretch of interest. Rather than attempt to correlate the OH stretching frequency with the many possible degrees of freedom in this system, we have, as described previously,[68] chosen to use only a single collective variable for our maps—the effective electric field $E$ at the location of the water hydrogen atom along the direction of the OH bond. For each configuration of water molecules, this electric field is computed from the point charges utilized in the molecular dynamics force field (excluding the molecule of interest). The DFT frequency for each cluster can then be plotted against $E$, and we can find a best-fit curve through the data points.[72] An alternate approach, however, is to determine the map $\omega(E)$ that will generate the correct distribution of DFT frequencies, $p(\omega)$, given the distribution of electric fields $P(E)$ in the liquid-state simulation. This "cumulative" map is calculated from[72]

$$\int_{\omega(E)}^{\infty} p(\omega')d\omega' = \int_{-\infty}^{E} P(E')\mathrm{d}E' \tag{3.1}$$

This approach shows clearly that the appropriate map is quadratic in the electric field,[72] which we then fit as such. This is the approach we pursue herein for $\omega_{10}$ and $\omega_{21}$. Note that although higher-order polynomials could also be used to fit the data, we have found that these more complicated maps do not result in any significant improvements. The dipole derivative $\mu'$ is also plotted against the electric field $E$, though in this case the map $\mu'(E)$ is determined using a quadratic least-squares fit to the data, constrained to pass through the calculated gas-phase monomer value.[75] The coordinate and momentum matrix elements correlate well with the DFT frequency, and our maps are thus linear fits to the data as a function of the frequency. For the case of intramolecular coupling, the map for $k_{jk}^{\text{intra}}$ was previously fit to a linear function of the sum of the electric fields for chromophores $j$ and $k$.[73] It should be noted that the $\mu'$ and $k_{jk}^{\text{intra}}$ maps are valid for both OH and OD spectroscopy.

A complete set of these revised and updated maps, parametrized from TIP4P bulk water simulations, are reported in Table 1. Note that some of these maps are identical to those published previously by us, while others have minor differences (these new calculations are based on more data points, with finer DVR grids). The number in square brackets to the right of each map indicates the root-mean-squared deviation (RMSD) between the maps and the DFT results. In each case, our spectroscopic maps qualitatively capture the general trends observed from the DFT calculations, though, as discussed

**Table 1. Spectroscopic Maps Parameterized from TIP4P Bulk Water Simulations**[a]

| | | |
|---|---|---|
| OH frequency, coordinate, and momentum maps | | |
| $\omega_{10} = 3760.2 - 3541.7E - 152677E^2$ | [63] | eq 3.4 |
| $\omega_{21} = 3606.0 - 3498.6E - 198715E^2$ | [76] | eq 3.5 |
| $x_{10} = 0.19285 - 1.7261 \times 10^{-5}\omega_{10}$ | $[1.7 \times 10^{-4}]$ | eq 3.6 |
| $x_{21} = 0.26836 - 2.3788 \times 10^{-5}\omega_{21}$ | $[3.0 \times 10^{-4}]$ | eq 3.7 |
| $p_{10} = 1.6466 + 5.7692 \times 10^{-4}\omega_{10}$ | $[4.5 \times 10^{-3}]$ | eq 3.8 |
| $p_{21} = 2.0160 + 8.7684 \times 10^{-4}\omega_{21}$ | $[8.3 \times 10^{-3}]$ | eq 3.9 |
| OD frequency, coordinate, and momentum maps | | |
| $\omega_{10} = 2767.8 - 2630.3E - 102601E^2$ | [45] | eq 3.10 |
| $\omega_{21} = 2673.0 - 1763.5E - 138534E^2$ | [52] | eq 3.11 |
| $x_{10} = 0.16593 - 2.0632 \times 10^{-5}\omega_{10}$ | $[1.5 \times 10^{-4}]$ | eq 3.12 |
| $x_{21} = 0.23167 - 2.8596 \times 10^{-5}\omega_{21}$ | $[2.7 \times 10^{-4}]$ | eq 3.13 |
| $p_{10} = 2.0475 + 8.9108 \times 10^{-4}\omega_{10}$ | $[5.3 \times 10^{-3}]$ | eq 3.14 |
| $p_{21} = 2.6233 + 13.1443 \times 10^{-4}\omega_{21}$ | $[9.5 \times 10^{-3}]$ | eq 3.15 |
| dipole derivative and intramolecular coupling maps | | |
| $\mu' = 0.1646 + 11.39E + 63.41E^2$ | [0.078] | eq 3.16 |
| $\omega_{jk}^{\text{intra}} = [-1361 + 27165(E_j + E_k)]x_j x_k - 1.887 p_j p_k$ | [180] | eq 3.17 |

[a]Root-mean-squared deviations (RMSD) for each map are shown in square brackets. Frequency maps, couplings, and associated RMSDs are given in units of wavenumbers, while the electric field $E$ and all other maps and associated RMSDs are given in atomic units.

previously, there is appreciable scatter in the data.[68] This scatter is primarily a result of the fact that the OH stretching frequency (and dipole derivative, etc.) is not a function only of the collective electric field variable $E$, but rather (within the Born-Oppenheimer approximation), it depends upon the nuclear positions of all of the surrounding water molecules. While we have found $E$ to be a reasonable proxy for the local solvation structure (and thus a good order parameter), it is not perfect. As such, we could, in principle, try to parametrize maps using multiple variables (e.g., the electric field at multiple positions or along several directions, or using electric field gradients[79−81]), but our previous attempts using this strategy have failed to decrease significantly the error associated with the maps. Alternatively, we could calculate the electric field $E$ not from the TIP4P point charges but from some other set of charges. This might involve scaling the TIP4P charges, as in a previous study of water in NaBr solutions,[77] or using fluctuating point charges to account for the polarizability of water. Though each of these generalizations may provide a future avenue for improvements in our methods, we have not pursued them herein.

Unlike the spectroscopic maps presented in Table 1, the intermolecular coupling between chromophores $j$ and $k$ on different molecules, eq 2.2, is a function not only of the electric fields $E_j$ and $E_k$ but also the relative orientation and distance between the OH (or OD) groups. If we assume only transition-dipole interactions,[25,95,69] then the second derivative of the potential energy surface $k_{jk}^{\text{intra}}$ is given by

$$k_{jk}^{\text{inter}} = \frac{\hat{u}_j\hat{u}_k - 3[(\hat{u}_j\hat{n}_{jk})(\hat{n}_{jk}\hat{u}_k)]}{r_{jk}^3}\mu'_j\mu'_k \tag{3.2}$$

where $\mu'_j$ is the dipole derivative for chromophore $j$, $\hat{u}_j$ is a unit vector along the direction of the transition dipole (along OH bond $j$), $\hat{n}_{jk}$ is a unit vector connecting the location of transition dipoles $j$ and $k$, and $r_{jk}$ is the distance between these transition-dipole locations. As described previously by Li et al.,[73] the only free parameter in eq 3.2 is the location of the transition dipole along the OH bond. This was previously fit based on DFT calculations of clusters of TIP4P bulk water, as described in section II, and it was found that the best-fit location for the transition dipole is 0.67 Å away from the water oxygen atom along the OH bond. We have elected not to refit this value, though as we demonstrated in ref 75., our updated maps for the dipole derivative $\mu'$ result in a significantly better fit for the intermolecular coupling than originally reported.[73]

As an example of the results of the fits of these maps, in the upper panel of Figure 1, we show the $\omega_{10}(E)$ OH-stretch map,

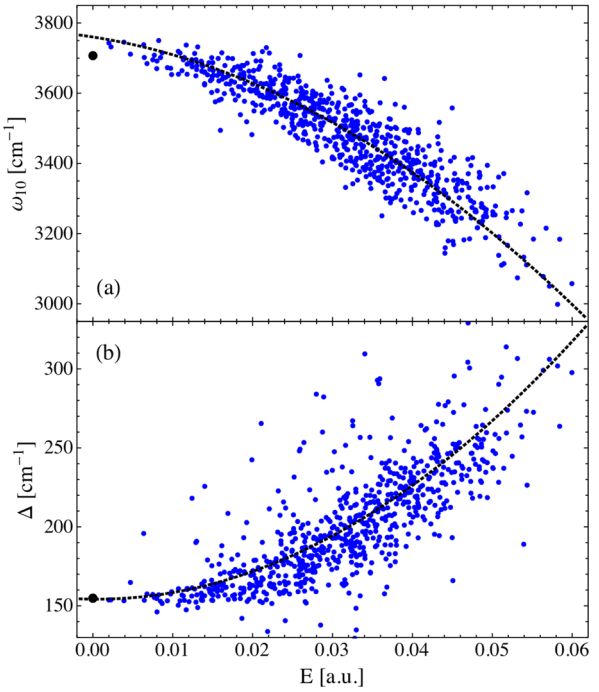


**Figure 1.** DFT calculations of the OH stretch fundamental frequency $\omega_{10}$ (a) and anharmonicity Δ (b) for water molecules from a TIP4P simulation of the bulk liquid versus the electric field $E$ (blue dots). The dotted black curves show the map results, eqs 3.4 and 3.5, and the black dot is the DFT result for the water monomer.

and also several hundred data points (out of around 2000) from the TIP4P liquid simulations. One sees that the fit to the data is reasonably good, although there is definitely some scatter. We could do the same for $\omega_{21}(E)$, but it is actually more interesting to consider the anharmonicity, defined by

$$\Delta \equiv \omega_{10} - \omega_{21} \tag{3.3}$$

This is shown in the bottom panel of Figure 1. As can be seen, the anharmonicity monotonically increases as the electric field (and thus the hydrogen-bond strength) increases. Note that for strong fields it is nearly double that of the monomer. The RMSD for the OH stretching anharmonicity is 30 cm$^{-1}$ (26 cm$^{-1}$ for OD)—smaller than the errors associated with either the 1−0 or 2−1 frequency maps individually.

## IV. ROBUSTNESS OF SPECTROSCOPIC MAPS

Given the set of spectroscopic maps presented in Table 1, in this section, we will examine the extent to which these maps can be applied to situations other than those for which the map was parametrized—water clusters taken from TIP4P bulk water simulations. Recently, we presented a newly parametrized force field for water that takes into account explicit three-body (E3B)

interactions between molecules.[83,84] This E3B force field was modified starting from the TIP4P force field and thus uses the same TIP4P point charges for electrostatic interactions. The model successfully reproduces many properties of bulk water, including the water diffusion coefficient, the H−H rotational correlation time, second and third virial coefficients, and the temperature dependence of the liquid density.[84] The E3B model has subsequently been utilized in our studies of the liquid/vapor interface, ice Ih, and the water hexamer.[21,75,76] For each of these cases, we have performed DFT calculations of the OH stretching frequency and transition dipole moment from water clusters chosen from the simulations. As described in section II, we investigate both bulk (E3B) water and the liquid/vapor interface at a temperature of 300 K, ice Ih at 10, 100, and 245 K, and the water hexamer at 80 and 194 K.

In Figure 2, we compare the frequency maps for the water OH stretch presented in Table 1, eqs 3.4 and 3.5, (black, dashed curve) to DFT calculations on water clusters chosen from E3B bulk water (blue dots), the liquid/vapor interface (orange), ice Ih at 100 K (green), and the water hexamer at 80 K (red). (Similar calculations (not shown) for ice Ih at 10 and 245 K and for the water hexamer at 194 K give qualitatively similar results.) The black dot at $E = 0$ indicates the calculated frequency of the gas-phase water monomer. Panel a plots the 1−0 frequency against electric field, as discussed in sction III, while the anharmonicity, eq 3.3, is plotted in panel b. Focusing first on the results for bulk liquid water (blue dots), one sees that the TIP4P-based map works about as well for E3B water as for TIP4P (Figure 1), which is to be expected (since as we said before the representative configurations are similar and the charge distributions in the two models are identical). Thus, we feel comfortable using this complete set of maps for E3B water. More surprisingly, from Figure 2, it is evident that the frequency and anharmonicity of water molecules in each of the other environments (surface, ice, hexamer) studied agree reasonably well with the TIP4P-parametrized spectroscopic maps. The scatter in the data points in Figure 2 for E3B bulk water, the surface, and the water hexamer are all similar in magnitude to the inherent scatter observed for TIP4P bulk liquid water.

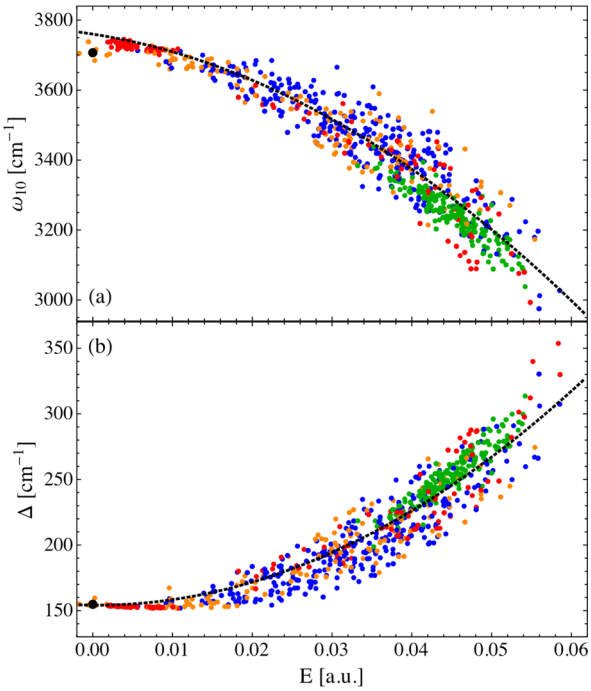


**Figure 2.** DFT calculations of the OH stretching frequency $\omega_{10}$ and anharmonicity Δ are compared to the TIP4P bulk water frequency maps, eqs 3.4 and 3.5, (black dashed curves) in panels a and b, respectively. Each dot corresponds to a cluster chosen from simulations of E3B bulk water (blue), the 80 K water hexamer (red), 100 K ice Ih (green), the water liquid/vapor interface (orange), and the gas-phase monomer (black).

A systematic shift in the calculated frequency relative to the map occurs for ice Ih (green dots). As all water molecules in ice have a very similar local environment, forming exactly four hydrogen bonds (leading to $4_D$−$4_D$ OH stretches in the language of Tainter et al.[82]), it is unsurprising that the DFT calculations are clustered in a relatively narrow band in both frequency and electric field (at 10 K, the distribution of points is even tighter). These points are systematically shifted to lower frequencies relative to the map by roughly 30 or 40 cm$^{-1}$. In addition, at values of $E > 0.05$ au, there are several DFT data points for both bulk water and the water hexamer that have frequencies less than 3000 cm$^{-1}$. These points invariably correspond to pairs of water molecules in a $3_S$−$3_D$ hydrogen-bonding arrangement—that is, the donor water molecule forms three hydrogen bonds and donates a single hydrogen bond to an acceptor water molecule that also forms three hydrogen bonds but is a double donor. As discussed by Tainter et al., this type of arrangement forms particularly strong hydrogen bonds, resulting in a very significant red-shift in the OH stretching frequency.[82,96] For both these very strong hydrogen bonds as well as for the $4_D$−$4_D$ hydrogen-bonding environments of ice, it appears as if our spectroscopic maps systematically overestimate the OH stretching frequency $\omega_{10}$.

In addition to frequency maps, we have also tested our dipole-derivative map and both the coordinate and momentum matrix−element maps for the same set of water clusters leading to the data in Figure 2. In Figure 3, the dipole derivative $\mu'$ is plotted against the electric field $E$, where the colored dots indicate DFT calculations for water in different environments, as in Figure 2, and the black, dashed curve is the dipole derivative map, eq 3.16, originally published in ref 75. As with the frequency maps, $\mu'$ for water in each environment we studied appears to match the TIP4P spectroscopic map

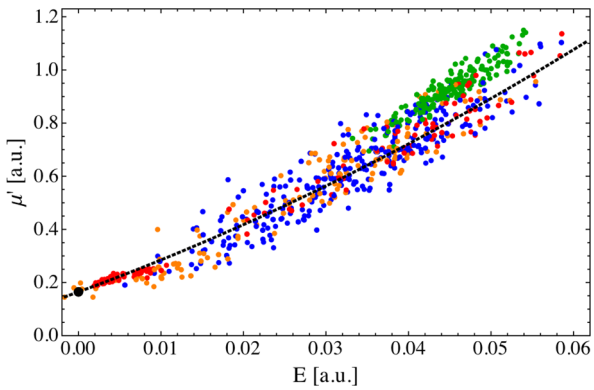


**Figure 3.** DFT calculations of the dipole derivative $\mu'$ for clusters from the same environments as in Figure 2 are compared to the TIP4P bulk water map, eq 3.16 (black dashed curve). The map is constrained to go through the gas-phase monomer value (black dot).


dx.doi.org/10.1021/ct400292q | J. Chem. Theory Comput. 2013, 9, 3109−3117

reasonably well, with higher electric fields (stronger hydrogen bonds) corresponding to a value of $\mu'$ that is up to a factor of 5 larger than the gas-phase value (black dot). Also, the calculations for ice Ih are systematically shifted to larger values of $\mu'$ relative to the map. Finally, note that, for every water environment investigated, the DFT calculations for the 1−0 and 2−1 coordinate and momentum matrix elements are in excellent agreement with our spectroscopic maps, eqs 3.6−3.9 and 3.12−3.15. As these maps show little scatter and no systematic shifts (even for ice), we have not plotted them here.

The calculation of spectroscopic observables for the case of neat $H_2O$ (or $D_2O$) requires both the intra- and intermolecular couplings between all of the OH (or OD) chromophores. The intramolecular coupling between chromophores $j$ and $k$, $\omega_{jk}^{intra}$, is related to the second derivative of the potential energy surface with respect to stretching each of these OH bonds, as well as the position and momentum matrix elements, as in eq 2.1. This second derivative $\omega_{jk}^{intra}$ is, in turn, roughly a linear function of the sum of the electric fields $E_j$ and $E_k$, as indicated in Table 1. In Figure 4, we compare this intramolecular coupling map, eq 3.17, to DFT data points for water clusters chosen from E3B bulk water, the water surface, ice Ih, the water hexamer, and the gas-phase monomer (blue, orange, green, red, and black, respectively). The dashed line indicates the diagonal. (Note that for the DFT data points, for this calculation we used the maps for the position and momentum matrix elements; since these are so slowly varying with $\omega_{10}$, the differences this produces are negligible.) In each case, the map does a good job of capturing the environmental dependence of $\omega_{jk}^{intra}$.

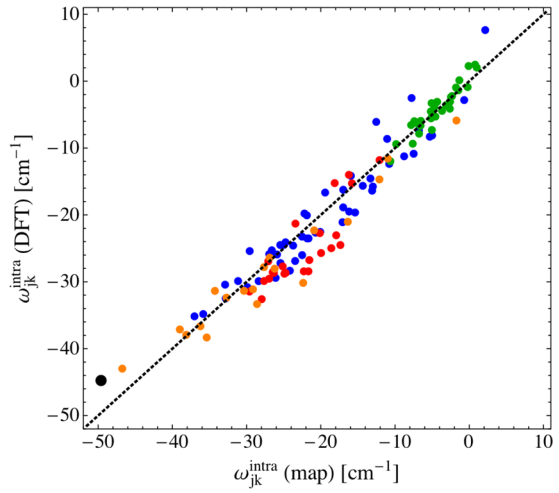


**Figure 4.** Comparison between the intramolecular coupling $\omega_{jk}^{intra}$ predicted by the TIP4P bulk water map, eq 3.17, and DFT calculations. The blue, red, orange, and green dots correspond to clusters chosen from E3B bulk water, the water hexamer at 80 K, the liquid/vapor interface, and ice Ih simulations at 100 K, respectively, and the black dot is the water monomer. The dashed line indicates the diagonal.

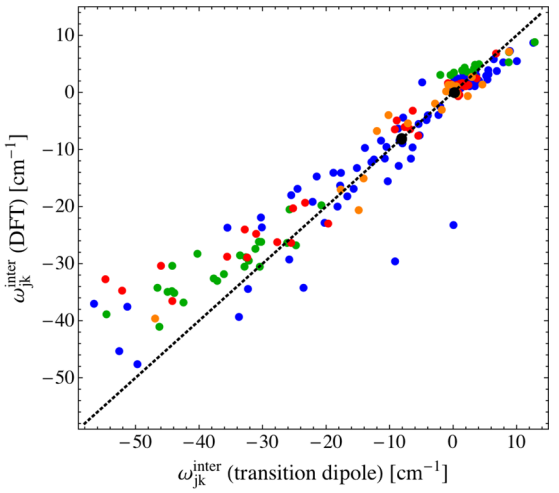


**Figure 5.** Comparison between the intermolecular coupling $\omega_{jk}^{intra}$ predicted by the transition dipole model, eq 3.2, and DFT calculations. The blue, red, orange, and green dots correspond to the same environments as in Figure 4, while the black dots correspond to the couplings in the gas-phase dimer. The dashed line indicates the diagonal.

It is interesting that the intramolecular couplings for the surface molecules are spread from 0 to almost −50 cm$^{-1}$, corresponding to a diversity of different environments at the surface. The liquid and cluster molecules have intermediate values of this coupling, around −20 cm$^{-1}$, while the ice molecule values are tightly clustered between 0 and −10 cm$^{-1}$. Thus, the intramolecular couplings in ice are essentially zero, which has profound implications for the vibrational spectroscopy (as we have discussed[75]—in particular, it implies that the molecular normal-mode basis is a poor one). An understanding of why this coupling nearly vanishes in ice comes from the map in eq 2.1: for the high electric fields in ice near 0.045 au, the potential term is positive and nearly cancels the negative kinetic term. In contrast, for the isolated $H_2O$ gas-phase monomer (where the electric fields are 0), the potential and kinetic terms are both negative and roughly equal, leading to a net overall substantial negative coupling. As shown in the figure, and as described in ref 74, our map predicts an intramolecular coupling of −49.6 cm$^{-1}$ for the monomer, as compared to the DFT value of −44.8 cm$^{-1}$ (and the experimental value of −49.4 cm$^{-1}$). We have also tested the effect of including more water molecules in our DFT calculations of the coupling (increasing the explicit cutoff discussed in section II), and we find that though additional waters do slightly alter the intramolecular couplings, the differences are typically only on the order of a few wavenumbers.

Finally, in Figure 5, we test the robustness of our transition-dipole intermolecular coupling map, eqs 2.2 and 3.2, for nearby water molecules in the same environments as in Figures 2−4. In Figure 5, however, the black dots correspond to the intermolecular couplings in the optimized E3B gas-phase water dimer. In the dimer, the data point near $\omega_{jk}^{intra} = 0$ corresponds to the coupling between two OH groups that are not involved in the intermolecular hydrogen bond, while the data point near $\omega_{jk}^{intra} = -10$ cm$^{-1}$ includes the OH group that forms the hydrogen bond. As was the case for the frequency, dipole derivative, and intramolecular coupling maps, our transition-dipole intermolecular coupling map reasonably accurately predicts the coupling between OH chromophores in bulk water, the surface, ice, and the water hexamer. For particularly strong couplings ($\omega_{jk}^{intra} < -30$ cm$^{-1}$), our transition-dipole map begins to differ significantly from the DFT results, and the magnitude of the coupling predicted by the map is somewhat larger than that found from our DFT calculations. Note that the "strong" intermolecular couplings in ice fall within this range.[75]

## V. CONCLUDING REMARKS

The spectroscopic maps used in previously reported studies of bulk water, the liquid/vapor interface, ice Ih, the water hexamer, and water interacting with other molecules[12,21,69,75−77] are all parametrized from water clusters chosen from bulk water simulations. Though these maps have allowed us to interpret and help understand experimental vibrational spectra, we had not carefully examined whether the bulk-water maps were appropriate for use with water in other environments. Therefore, in this article, we have tested the robustness of spectroscopic maps for the water OH (and OD) stretching frequencies, transition dipoles, and couplings for different water environments. In each case, we find that the maps parametrized from bulk water simulations perform well and thus are useful for studies of, for example, ice or water clusters.

There are a few systematic trends that are worth commenting on. The 1−0 transition frequencies from the map are systematically too high for ice, by about 30 or 40 $cm^{-1}$, indicative of the (unsurprising) fact that ice configurations are not representative of liquid water. Morever, the dipole-derivative map is systematically too low for ice. Finally, for all systems the magnitude of the intermolecular coupling from the dipole approximation is too large by perhaps 10 $cm^{-1}$ for pairs of OH stretches that are strongly coupled. In particular, this is true for the "strong intermolecular coupling pairs" in ice.[75] Perhaps this is also not too surprising, since these are the closest pairs, and so, the dipole−dipole approximation might be expected to begin to break down. These deficiencies all have consequences for ice spectroscopy. A more accurate frequency map would red-shift the theoretical frequencies, bringing theory in closer agreement with experiment.[75] A more accurate intermolecular coupling map would decrease the magnitude of the coupling, whereas a more accurate dipole-derivative map would tend to increase the magnitude of the coupling, so perhaps these two effects would more or less cancel. In any case, one could imagine developing specialized maps for each particular water situation (such as in ice). However, our feeling is that the appeal and generality of a universal set of maps may outweigh the benefits of marginally improved accuracy using more specialized maps.

There are, of course, other limitations and issues involved with our approaches—to name a few: treating the low-frequency motions, especially the librations, classically; neglecting coupling to the bend overtone,[97] using a one-dimensional collective coordinate, using DFT for the electronic-structure calculations, and using a one-dimensional pseudodiatomic approximation for the local-mode frequencies. Perhaps it would be useful to pursue some of these issues in lieu of tweaking the specifics of the maps. Ultimately, we are interested in using the E3B model in conjunction with other species (ions, solutes, biomolecules, etc.). So, at some point, it will also be important to test the validity of the maps for these more general situations.

One interesting point worth discussing involves the reason for the considerable success of the map approach. For example, in considering the local-mode OH-stretch frequencies, we have discussed how the enormous frequency shifts (from the gas-phase value) arise from complicated and cooperative charge-transfer and electronic-structure effects[98] involving hydrogen-bonding in donor−acceptor pairs.[82] To summarize: Consider a donor−acceptor hydrogen-bonded pair, as shown schematically in Figure 6 (the donor H atom is shown in red). From an electronic-structure point of view, the red-shift of the donor

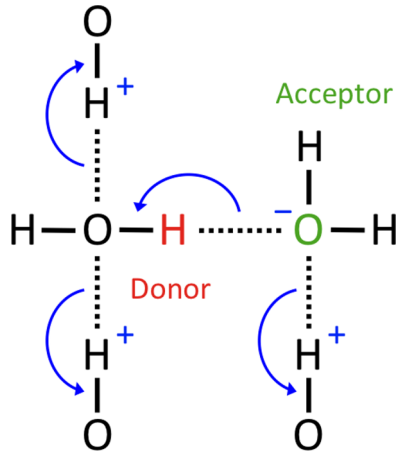


**Figure 6.** Schematic of a donor−acceptor hydrogen-bonded pair of water molecules. The donor H atom is in red, and the acceptor O atom is in green. Two acceptor hydrogen bonds on the donor molecule, and one additional acceptor hydrogen bond on the acceptor molecule are also shown. The blue arrows indicate charge transfer from oxygen lone-pair electrons to OH $\sigma^*$ orbitals, while + and − indicate partial charges on the relevant O and H atoms.

OH frequency comes in part from a small amount of charge transfer (indicated by the arrow) from the lone pairs of the acceptor oxygen (shown in green) to the $\sigma^*$ orbital of the donor OH bond, causing a weakening of the bond and a red-shift of the donor OH-stretch frequency. We have argued (also see Ohno et al.[96]) that one or two additional acceptor hydrogen bonds made by the donor molecule (shown schematically in the figure) lead to a significantly larger red-shift of the donor OH stretch, due to charge transfer away from the donor molecule, facilitating additional charge transfer from the acceptor molecule. On the other hand, an additional acceptor hydrogen bond made by the acceptor molecule (also shown in the figure) leads to a blue-shift of the donor OH stretch, since in this case charge transfer is away from acceptor molecule, leaving less electron density for charge transfer to the donor molecule.

How are the effects of complicated electronic structure captured by a scalar electric field? The explanation is also shown schematically in the figure. Within the map approach, the red-shift of the donor OH stretch as a result of the hydrogen bond to the acceptor molecule is due to a reasonably strong electric field from the (negatively charged) acceptor oxygen at the donor hydrogen (and projected along the donor OH bond). Additional acceptor hydrogen bonds on the donor molecule enhance this field (from the positively charged H atoms, as shown schematically in the figure), leading to a larger red-shift. An additional acceptor hydrogen bond on the acceptor molecule depletes this field (again, from a positively charged H atom), causing a blue shift. Admittedly, none of this was understood or anticipated when the maps were originally developed,[67,68] but on reflection, this appears to be the explanation. In conclusion, herein we show that our simple and universal electric-field maps are quite useful for studying water in a variety of situations, and we have some idea as to why they work as well as they do.

## AUTHOR INFORMATION


### Corresponding Author

*E-mail: scott.m.gruenbaum@gmail.com.


### Notes

The authors declare no competing financial interest.

## ACKNOWLEDGMENTS

This work was primarily supported through by the National Science Foundation through Grant No. CHE-1058752. Additional computational time for calculations of coupling maps was supported in part by NSF Grant No. CHE-0840494.

## REFERENCES


(1) Rog, T.; Murzyn, K.; Pasenkiewicz-Gierula, M. *Chem. Phys. Lett.* **2002**, *352*, 323−327.
(2) Sykora, J.; Jurkiewicz, P.; Epand, R. M.; Kraayenhof, R.; Langner, M.; Hof, M. *Chem. Phys. Lipids* **2005**, *135*, 213−221.
(3) Bhide, S. Y.; Berkowitz, M. L. *J. Chem. Phys.* **2005**, *123*, 224702.
(4) Murzyn, K.; Zhao, W.; Karttunen, M.; Kurdziel, M.; Rog, T. *Biointerphases* **2006**, *1*, 98−105.
(5) Moilanen, D. E.; Levinger, N. E.; Spry, D. B.; Fayer, M. D. *J. Am. Chem. Soc.* **2007**, *129*, 14311−14318.
(6) Moilanen, D. E.; Piletic, I. R.; Fayer, M. D. *J. Phys. Chem. C* **2007**, *111*, 8884−8891.
(7) Zhao, W.; Moilanen, D. E.; Fenn, E. E.; Fayer, M. D. *J. Am. Chem. Soc.* **2008**, *130*, 13927−13937.
(8) Ball, P. *Chem. Rev.* **2008**, *108*, 74−108.
(9) van Meer, G.; Voelker, D. R.; Feigenson, G. W. *Mol. Cell Biol.* **2008**, *9*, 112−124.
(10) Zhang, Z.; Berkowitz, M. L. *J. Phys. Chem. B* **2009**, *113*, 7676−7680.
(11) Zhong, D.; Pal, S. K.; Zewail, A. H. *Chem. Phys. Lett.* **2011**, *503*, 1−11.
(12) Gruenbaum, S. M.; Skinner, J. L. *J. Chem. Phys.* **2011**, *135*, 075101.
(13) Gruenbaum, S. M.; Pieniazek, P. A.; Skinner, J. L. *J. Chem. Phys.* **2011**, *135*, 164506.
(14) Taylor, R. S.; Dang, L. X.; Garrett, B. C. *J. Phys. Chem.* **1996**, *100*, 11720−11725.
(15) Liu, P.; Harder, E.; Berne, B. J. *J. Phys. Chem. B* **2004**, *108*, 6595−6602.
(16) Kuo, I.-F. W.; Mundy, C. J. *Science* **2004**, *303*, 658−660.
(17) Kuo, I.-F. W.; Mundy, C. J.; Eggimann, B. L.; McGrath, M. J.; Siepmann, J. I.; Chen, B.; Vieceli, J.; Tobias, D. J. *J. Phys. Chem. B* **2006**, *110*, 3738−3746.
(18) Kühne, T. D.; Pascal, T. A.; Kaxiras, E.; Jung, Y. *J. Phys. Chem. Lett.* **2011**, *2*, 105−113.
(19) Verde, A. V.; Bolhuis, P. G.; Campen, R. K. *J. Phys. Chem. B* **2012**, *116*, 9467−9481.
(20) Chakraborty, D.; Chandra, A. *Chem. Phys.* **2012**, *392*, 96−104.
(21) Ni, Y.; Gruenbaum, S. M.; Skinner, J. L. *Proc. Natl. Acad. Sci. U.S.A.* **2013**, *110*, 1992−1998.
(22) Fecko, C. J.; Eaves, J. D.; Loparo, J. J.; Tokmakoff, A.; Geissler, P. L. *Science* **2003**, *301*, 1698−1702.
(23) Nibbering, E. T. J.; Elsaesser, T. *Chem. Rev.* **2004**, *104*, 1887−1914.
(24) Fecko, C. J.; Loparo, J. J.; Roberts, S. T.; Tokmakoff, A. *J. Chem. Phys.* **2005**, *122*, 054506.
(25) Buch, V. *J. Phys. Chem. B* **2005**, *109*, 17771−17774.
(26) Bakker, H.; Skinner, J. L. *Chem. Rev.* **2010**, *110*, 1498−1517.
(27) Asbury, J. B.; Steinel, T.; Stromberg, C.; Corcelli, S. A.; Lawrence, C. P.; Skinner, J. L.; Fayer, M. D. *J. Phys. Chem. A* **2004**, *108*, 1107−1119.
(28) Asbury, J. B.; Steinel, T.; Kwak, K.; Corcelli, S. A.; Lawrence, C. P.; Skinner, J. L.; Fayer, M. D. *J. Chem. Phys.* **2004**, *121*, 12431−12446.
(29) Loparo, J. J.; Roberts, S. T.; Tokmakoff, A. *J. Chem. Phys.* **2006**, *125*, 194521.
(30) Loparo, J. J.; Roberts, S. T.; Tokmakoff, A. *J. Chem. Phys.* **2006**, *125*, 194522.
(31) Roberts, S. T.; Ramasesha, K.; Tokmakoff, A. *Acc. Chem. Res.* **2009**, *42*, 1239−1249.
(32) Nicodemus, R. A.; Ramasesha, K.; Roberts, S. T.; Tokmakoff, A. *J. Phys. Chem. Lett.* **2010**, *1*, 1068−1072.
(33) Ramasesha, K.; Roberts, S. T.; Nicodemus, R. A.; Mandal, A.; Tokmakoff, A. *J. Chem. Phys.* **2011**, *135*, 054509.
(34) Nicodemus, R. A.; Corcelli, S. A.; Skinner, J. L.; Tokmakoff, A. *J. Phys. Chem. B* **2011**, *115*, 5604−5616.
(35) Jansen, T. L. C.; Auer, B. M.; Yang, M.; Skinner, J. L. *J. Chem. Phys.* **2010**, *132*, 224503.
(36) Woutersen, S.; Bakker, H. J. *Nature* **1999**, *402*, 507−509.
(37) Cringus, D.; Jansen, T. L. C.; Pshenichnikov, M. S.; Wiersma, D. A. *J. Chem. Phys.* **2007**, *127*, 084507.
(38) Moilanen, D. E.; Fenn, E. E.; Lin, Y.-S.; Skinner, J. L.; Bagchi, B.; Fayer, M. D. *Proc. Natl. Acad. Sci. U.S.A.* **2008**, *105*, 5295−5300.
(39) Piatkowski, L.; Eisenthal, K. B.; Bakker, H. J. *Phys. Chem. Chem. Phys.* **2009**, *11*, 9033−9038.
(40) Lin, Y.-S.; Pieniazek, P. A.; Yang, M.; Skinner, J. L. *J. Chem. Phys.* **2010**, *132*, 174505.
(41) Piatkowski, L.; de Heij, J.; Bakker, H. J. *J. Phys. Chem. B* **2013**, *117*, 1367−1377.
(42) Laage, D.; Stirnemann, G.; Sterpone, F.; Rey, R.; Hynes, J. T. *Annu. Rev. Phys. Chem.* **2011**, *62*, 395−416.
(43) Laage, D.; Stirnemann, G.; Sterpone, F.; Hynes, J. T. *Acc. Chem. Res.* **2012**, *45*, 53−62.
(44) Richmond, G. L. *Chem. Rev.* **2002**, *102*, 2693−2724.
(45) Shen, Y. R.; Ostroverkhov, V. *Chem. Rev.* **2006**, *106*, 1140−1154.
(46) Ostroverkhov, V.; Waychunas, G. A.; Shen, Y. R. *Phys. Rev. Lett.* **2005**, *94*, 046102.
(47) Tian, C.-S.; Shen, Y. R. *J. Am. Chem. Soc.* **2009**, *131*, 2790−2791.
(48) Pieniazek, P. A.; Tainter, C. J.; Skinner, J. L. *J. Am. Chem. Soc.* **2011**, *133*, 10360−10363.
(49) Sovago, M.; Campen, R. K.; Wurpel, G. W. H.; Müller, M.; Bakker, H. J.; Bonn, M. *Phys. Rev. Lett.* **2008**, *100*, 173901.
(50) Sovago, M.; Campen, R. K.; Bakker, H. J.; Bonn, M. *Chem. Phys. Lett.* **2009**, *470*, 7−12.
(51) Pieniazek, P. A.; Tainter, C. J.; Skinner, J. L. *J. Chem. Phys.* **2011**, *135*, 044701.
(52) Yang, M.; Li, F.; Skinner, J. L. *J. Chem. Phys.* **2011**, *135*, 164505.
(53) Fenn, E. E.; Fayer, M. D. *J. Chem. Phys.* **2011**, *135*, 074502.
(54) Vacha, R.; Siu, S. W. I.; Petrov, M.; Bockmann, R. A.; Barucha-Kraszewska, J.; Jurkiewicz, P.; Hof, M.; Berkowitz, M. L.; Jungwirth, P. *J. Phys. Chem. A* **2009**, *113*, 7235−7243.
(55) Broemstrup, T.; Reuter, N. *Biophys. J.* **2010**, *99*, 825−833.
(56) Sharp, K. A.; Vanderkooi, J. M. *Acc. Chem. Res.* **2010**, *43*, 231−239.
(57) Yagasaki, T.; Saito, S. *J. Chem. Phys.* **2011**, *135*, 244511.
(58) Yang, L.; Fan, Y.; Gao, Y. Q. *J. Phys. Chem. B* **2011**, *115*, 12456−12465.
(59) Aragones, J. L.; Sanz, E.; Vega, C. *J. Chem. Phys.* **2012**, *136*, 244508.
(60) McBride, C.; Noya, E. G.; Aragones, J. L.; Conde, M. M.; Vega, C. *Phys. Chem. Chem. Phys.* **2012**, *14*, 10140−10146.
(61) Galamba, N. *J. Phys. Chem. B* **2012**, *116*, 5242−5250.
(62) Skinner, J. L.; Auer, B. M.; Lin, Y.-S. *Adv. Chem. Phys.* **2009**, *142*, 59−103.
(63) Rice, S.; Bergren, M.; Belch, A.; Nielson, N. *J. Phys. Chem.* **1983**, *87*, 4295−4308.
(64) Buch, V.; Tarbuck, T.; Richmond, G. L.; Groenzin, H.; Li, I.; Schultz, M. J. *J. Chem. Phys.* **2007**, *127*, 204710.
(65) Mukamel, S. *Principles of Nonlinear Optical Spectroscopy*; Oxford: New York, 1995; p 111−141.
(66) Hermansson, K.; Knuts, S.; Lindgren, J. *J. Chem. Phys.* **1991**, *95*, 7486−7496.

(67) Corcelli, S. A.; Lawrence, C. P.; Skinner, J. L. *J. Chem. Phys.* **2004**, *120*, 8107−8117.
(68) Auer, B. M.; Kumar, R.; Schmidt, J. R.; Skinner, J. L. *Proc. Natl. Acad. Sci. U.S.A.* **2007**, *104*, 14215−14220.
(69) Auer, B. M.; Skinner, J. L. *J. Chem. Phys.* **2008**, *128*, 224511.
(70) Yang, M.; Skinner, J. L. *J. Chem. Phys.* **2011**, *135*, 154114.
(71) Jansen, T. L. C.; Cringus, D.; Pshenichnikov, M. S. *J. Phys. Chem. A* **2009**, *113*, 6260−6265.
(72) Li, F.; Skinner, J. L. *J. Chem. Phys.* **2010**, *132*, 204505.
(73) Li, F.; Skinner, J. L. *J. Chem. Phys.* **2010**, *133*, 244504.
(74) Li, F.; Skinner, J. L. *J. Chem. Phys.* **2011**, *134*, 099901.
(75) Shi, L.; Gruenbaum, S. M.; Skinner, J. L. *J. Phys. Chem. B* **2012**, *116*, 13821−13830.
(76) Tainter, C. J.; Skinner, J. L. *J. Chem. Phys.* **2012**, *137*, 104304.
(77) Lin, Y.-S.; Auer, B. M.; Skinner, J. L. *J. Chem. Phys.* **2009**, *131*, 144511.
(78) Pieniazek, P. A.; Lin, Y.-S.; Chowdhary, J.; Ladanyi, B. M.; Skinner, J. L. *J. Phys. Chem. B* **2009**, *113*, 15017−15028.
(79) Hayashi, T.; Jansen, T. L. C.; Zhuang, W.; Mukamel, S. *J. Phys. Chem. A* **2005**, *109*, 64−82.
(80) Paarmann, A.; Hayashi, T.; Mukamel, S.; Miller, R. J. D. *J. Chem. Phys.* **2008**, *128*, 191103.
(81) Paarmann, A.; Hayashi, T.; Mukamel, S.; Miller, R. J. D. *J. Chem. Phys.* **2009**, *130*, 204110.
(82) Tainter, C. J.; Ni, Y.; Shi, L.; Skinner, J. L. *J. Phys. Chem. Lett.* **2013**, *4*, 12−17.
(83) Kumar, R.; Skinner, J. L. *J. Phys. Chem. B* **2008**, *112*, 8311−8318.
(84) Tainter, C. J.; Pieniazek, P. A.; Lin, Y.-S.; Skinner, J. L. *J. Chem. Phys.* **2011**, *134*, 184501.
(85) Jorgensen, W. L.; Chandrasekhar, J.; Madura, J. D.; Impey, R. W.; Klein, M. L. *J. Chem. Phys.* **1983**, *79*, 926−935.
(86) Lindahl, E.; Hess, B.; van der Spoel, D. *J. Mol. Model.* **2001**, *7*, 306−317.
(87) Hoover, W. G. *Phys. Rev. A* **1985**, *31*, 1695−1697.
(88) Parrinello, M.; Rahman, A. *J. Chem. Phys.* **1982**, *76*, 2662−2666.
(89) Essmann, U.; Perera, L.; Berkowitz, M. L.; Darden, T.; Lee, H.; Pedersen, L. G. *J. Chem. Phys.* **1995**, *103*, 8577−8593.
(90) Frisch, M. J.; Trucks, G. W.; Schlegel, H. B.; Scuseria, G. E.; Robb, M. A.; Cheeseman, J. R.; Montgomery, J. A., Jr.; Vreven, T.; Kudin, K. N.; Burant, J. C.; Millam, J. M.; Iyengar, S. S.; Tomasi, J.; Barone, V.; Mennucci, B.; Cossi, M.; Scalmani, G.; Rega, N.; Petersson, G. A.; Nakatsuji, H.; Hada, M.; Ehara, M.; Toyota, K.; Fukuda, R.; Hasegawa, J.; Ishida, M.; Nakajima, T.; Honda, Y.; Kitao, O.; Nakai, H.; Klene, M.; Li, X.; Knox, J. E.; Hratchian, H. P.; Cross, J. B.; Bakken, V.; Adamo, C.; Jaramillo, J.; Gomperts, R.; Stratmann, R. E.; Yazyev, O.; Austin, A. J.; Cammi, R.; Pomelli, C.; Ochterski, J. W.; Ayala, P. Y.; Morokuma, K.; Voth, G. A.; Salvador, P.; Dannenberg, J. J.; Zakrzewski, V. G.; Dapprich, S.; Daniels, A. D.; Strain, M. C.; Farkas, O.; Malick, D. K.; Rabuck, A. D.; Raghavachari, K.; Foresman, J. B.; Ortiz, J. V.; Cui, Q.; Baboul, A. G.; Clifford, S.; Cioslowski, J.; Stefanov, B. B.; Liu, G.; Liashenko, A.; Piskorz, P.; Komaromi, I.; Martin, R. L.; Fox, D. J.; Keith, T.; Al-Laham, M. A.; Peng, C. Y.; Nanayakkara, A.; Challacombe, M.; Gill, P. M. W.; Johnson, B.; Chen, W.; Wong, M. W.; Gonzalez, C.; Pople, J. A. *Gaussian 03*, Gaussian Inc., Pittsburgh PA, 2003.
(91) Stephens, P. J.; Devlin, F. J.; Chabalowski, C. F.; Frisch, M. J. *J. Phys. Chem.* **1994**, *98*, 11623−11627.
(92) Burns, L. A.; Vazquez-Mayagoitia, A.; Sumpter, B. G.; Sherrill, C. D. *J. Chem. Phys.* **2011**, *134*, 084107.
(93) Colbert, D.; Miller, W. H. *J. Chem. Phys.* **1992**, *96*, 1982−1991.
(94) Benedict, W. S.; Gailar, N.; Plyler, E. K. *J. Chem. Phys.* **1956**, *24*, 1139−1165.
(95) Torii, H. *J. Phys. Chem. A* **2006**, *110*, 4822−4832.
(96) Ohno, K.; Okimura, M.; Akai, N.; Katsumoto, Y. *Phys. Chem. Chem. Phys.* **2005**, *7*, 3005−3014.
(97) Liu, H.; Wang, Y.; Bowman, J. M. *J. Phys. Chem. Lett.* **2012**, *3*, 3671−3676.
(98) Weinhold, F.; Landis, C. *Valency and Bonding: A Natural Bond Orbital Donor-Acceptor Perspective*; Cambridge University Press: Cambridge, 2005; pp 593−660.